



Cardiac Displacement Tracking with Data Assimilation Combining a Biomechanical Model and an Automatic Contour Detection

Radomír Chabiniok^{1,2,3}, Gautier Bureau^{1,2}, Alexandra Groth⁴,
Jaroslav Tintera⁵, Jürgen Weese⁴, Dominique Chapelle^{1,2},
and Philippe Moireau^{1,2}(✉)

¹ Inria, Université Paris-Saclay, Palaiseau, France
philippe.moireau@inria.fr

² LMS, Ecole Polytechnique, CNRS, Université Paris-Saclay, Palaiseau, France

³ School of Biomedical Engineering and Imaging Sciences (BMEIS),
St Thomas' Hospital, King's College London, London, UK

⁴ Philips, Research Laboratories, Hamburg, Germany

⁵ Institute for Clinical and Experimental Medicine, Prague, Czech Republic

Abstract. Data assimilation in computational models represents an essential step in building patient-specific simulations. This work aims at circumventing one major bottleneck in the practical use of data assimilation strategies in cardiac applications, namely, the difficulty of formulating and effectively computing adequate data-fitting term for cardiac imaging such as cine MRI. We here provide a proof-of-concept study of data assimilation based on automatic contour detection. The tissue motion simulated by the data assimilation framework is then assessed with displacements extracted from tagged MRI in six subjects, and the results illustrate the performance of the proposed method, including for circumferential displacements, which are not well extracted from cine MRI alone.

Keywords: Biophysical heart modeling · Data assimilation · cine MRI

1 Introduction

It is now widely accepted that data assimilation strategies are the fundamental ingredient for personalizing biophysical cardiac models, as they have the capability to decrease the discrepancy between model and data, while estimating values of key biophysical parameters [2]. However, one major limitation in the practical use of such modeling and data assimilation strategies in clinical applications lies in the difficulty of formulating and effectively computing adequate data-fitting terms, especially where imaging data are concerned. In some specific imaging techniques such as tagged MRI, displacements fields can be extracted

from image sequences [5, 16], in which case comparison with models is straightforward, but the question arises of assessing the accuracy of these extracted displacements. However, for more standard image data such as cine MRI, CT, or ultrasound, data processing does not readily provide such displacements fields. Some previous proof-of-concept works have successfully used pre-segmented cine MR images [1] with data-fitting terms based on distances between the simulated model boundaries and the segmentation contours [1, 9, 13]. The segmentation itself however represents an additional step that complexifies the data assimilation pipeline – with possible additional errors. Our objective here is to use a previously-proposed method for automatic contour detection [4] in cardiac images to design an integrated data-fitting term in a complete data assimilation framework with a cardiac biomechanical model.

2 Methods

The section presents the clinical data, the biophysical model, the cine MRI data-fitting term, the data assimilation method, and the assessment strategy based on tagged MRI.

2.1 Clinical Data

Four healthy volunteers and two patients with a suspected cardiomyopathy were involved in the study as *test subjects*. For each subject, the following MR cardiac images were acquired by using a Philips Achieva 1.5T MR system (for healthy volunteers), and Siemens Aera 1.5T (for the patients):

- Time-resolved cine MRI (multiple 2D cine bSSFP) in breath-hold and retrospective ECG gating, with the following parameters: temporal resolution 25–30 ms, field of view (FOV) 350×350 mm, parallel imaging using acceleration factor of 2, acquired spatial resolution $\sim 2.3 \times 2.3 \times 8$ mm (inter-slice spacing 10 mm).
- Tagged MRI in prospective ECG triggering: 3D tagged MRI [16] for Philips scanner (FOV $100 \times 100 \times 100$ mm, spatial resolution $3.4 \times 7.7 \times 7.7$ mm, temporal resolution ~ 35 ms); 2D tagged (CSPAMM) for Siemens scanner for which 3D tagged sequence was not available (FOV 350×350 mm, spatial resolution $3 \times 3 \times 7$ mm, temporal resolution ~ 35 ms).
- Whole-heart 3D bSSFP sequence [6] acquired in free breathing by using breath-navigator, acquisition matrix $212 \times 209 \times 200$, acquired voxel size $2 \times 2 \times 2$ mm, repetition time 4.5 ms, echo time 2.2 ms, echo train length 26 and flip angle 90° .

In addition, cine MRI together with the 3D whole-heart sequence was acquired in ten *training subjects* (with Philips Achieva 1.5 T scanner). The training group included five healthy volunteers and five patients with dilated cardiomyopathy. There was no intersection between the *test* and *training* groups.

Cine sequences covered the whole ventricles by a set of parallel short-axis (SA) slices (the so-called “SA cine stack” or “SA stack”). Spatial mis-registration of the slices within the SA cine stack (caused by acquiring the stack in 5–15 breath-hold periods) was corrected by the rigid registration function from the Image Registration Toolkit IRTK [18], while using the high-resolution 3D whole-heart image as a template.

2.2 Biomechanical Heart Model

Any data assimilation procedure relies on an underlying physical model. By this, we mean a patient-specific geometry with additional microstructure information such as the myocardial fiber directions, but also a mechanical formulation combining a constitutive law and boundary conditions in a continuum mechanics framework.

Geometry – A biventricular geometry is obtained by manual segmentation of the end-diastolic time frame of the SA cine MR stack of images covering the whole heart. The segmentation produces a surface triangle mesh $\Gamma_0^{h,k}$, $1 \leq k \leq 6$ where k denotes the subject number, and h means that this is a meshed surface. Then, a tetrahedral mesh $\Omega_0^{h,k}$ is generated from the boundary using the GHS3D software¹, namely such that $\partial\Omega_0^{h,k} = \Gamma_0^{h,k}$. The myocardial fiber directions $\boldsymbol{\tau}$ are prescribed analytically at each integration point of the volume mesh according to a rule-based criterion with the elevation angle being $-60/60^\circ$ for the LV (from epicardium to endocardium) and $-75/75^\circ$ for RV. Note that defining the reference configuration from an initial geometry can be improved by solving a static mechanical equilibrium involving the passive constitutive law and an internal ventricular pressure, see [15] and references therein.

Biomechanical Model – We rely on the biomechanical model described in [3]. We consider a total Lagrangian formulation allowing to compute at every time t the deformation mapping $\boldsymbol{\varphi}$ with respect to the reference configuration $\Omega_0^{h,k}$, namely

$$\boldsymbol{\varphi} : \left\{ \begin{array}{l} \Omega_0^{h,k} \rightarrow \Omega_{h,k}(t) \\ \mathbf{x} \mapsto \mathbf{x}(t) = \boldsymbol{\varphi}(\mathbf{x}, t) = \mathbf{x} + \mathbf{u}(\mathbf{x}, t) \end{array} \right.$$

where \mathbf{u} stands for the displacement field. We recall the following kinematics tensors definitions: the deformation gradient $\mathbf{F} = \nabla \mathbf{u}$ with J its determinant, the right Cauchy-Green deformation tensor $\mathbf{C} = \mathbf{F}^\top \cdot \mathbf{F}$ and $\mathbf{e} = \frac{1}{2}(\mathbf{C} - \mathbf{1})$ the Green-Lagrange strain tensor. The constitutive law defining the second Piola-Kirchhoff stress tensor $\boldsymbol{\Sigma}$ consists of an active part – based on Huxley’s law – along the fiber directions $\sigma_a(\mathbf{F}, t)\boldsymbol{\tau}(\mathbf{x}) \otimes \boldsymbol{\tau}(\mathbf{x})$, a hyperelastic part $\boldsymbol{\Sigma}^p(\mathbf{C})$ and a viscoelastic part $\boldsymbol{\Sigma}^v(\partial_t \mathbf{C}, \mathbf{C})$ [3]. The heart geometry is fixed on the apex and anterior wall (simplifying the contact between epicardium and thorax and diaphragm)

¹ Inria, Project-Team Gamma.

by using visco-elastic boundary conditions with stiffness and viscosity parameters α, β [13]. Similar albeit more compliant boundary conditions are prescribed at the basal boundary as a substitute for atria and large vessels. Finally, the systemic and pulmonary circulations are modeled by Windkessel models, each containing a combination of proximal and distal resistance-capacitance systems [17]. A valve model connects the left and right ventricular pressures $p_{v,i}$ to the systemic and pulmonary circulations [17], respectively. The principle of virtual work in the space of admissible test displacements \mathcal{V}_{ad} reads

$$\int_{\Omega_0^{h,k}} \rho \partial_{tt} \mathbf{u} \cdot \mathbf{w} \, d\Omega + \int_{\Omega_0^{h,k}} \boldsymbol{\Sigma} : \text{De}[\mathbf{u}](\mathbf{w}) \, d\Omega + \int_{\Gamma_{0,b}^{h,k}} (\alpha \mathbf{u} + \beta \partial_t \mathbf{u}) \cdot \mathbf{w} \, d\Gamma = - \sum_{i=l,r} \int_{\Gamma_{0,\text{endo}_i}^{h,k}} p_{v,i} \mathcal{J} \mathbf{F}^{-1} \mathbf{n} \cdot \mathbf{w} \, d\Gamma, \quad \mathbf{w} \in \mathcal{V}_{\text{ad}},$$

where $\text{De}[\mathbf{u}]$ denotes the differential of the strain tensor \mathbf{e} around the displacement \mathbf{u} and \mathbf{n} the outward unit normal vector. The model is discretized in time using a Newmark scheme and in space using finite elements. It is implemented in the MPI-based MoReFEM library² and we follow [1] to pre-calibrate the model to patients’ data.

2.3 Distance Computation in Cine MRI

In order to provide a data-fitting term directly based on cine MRI, we use the framework of [4, 14] – trained using all ten *training* subjects – to detect endo- and epicardial boundaries in the SA cine images. Then, for any computed deformation $\boldsymbol{\varphi}(\mathbf{x}, t)$, the boundary detection mechanism is used to find target points in the image for each triangle $\mathcal{T}^{h,k}$ from the endo- $\Gamma_{\text{endo}_i}^{h,k}(t)$, $i = l, r$, and epicardial $\Gamma_{\text{epi}_i}^{h,k}(t)$ surfaces of the deformed model. From these target points, we can compute a signed distance between all points of $\Gamma_{\text{ext}}^{h,k}(t) = \cup_{i=l,r} \Gamma_{\text{endo}_i}^{h,k}(t) \cup \Gamma_{\text{epi}_i}^{h,k}(t)$ and the target points $\mathbf{x}_{\text{Im}}(\mathcal{T}^{h,k}(\mathbf{x}))$.

$$\text{dist}_{\text{Im}} : \begin{cases} \Gamma_{\text{ext}}^{h,k}(t) \rightarrow \mathbb{R}^3 \\ \mathbf{x} \mapsto \mathbf{x}_{\text{Im}}(\mathcal{T}^{h,k}(\mathbf{x})) - \mathbf{x} \end{cases}$$

Note that this signed distance contains (1) the information of being in or out of the mesh boundaries, (2) the distance itself $\|\mathbf{x}_{\text{Im}}(\mathcal{T}^{h,k}(\mathbf{x})) - \mathbf{x}\|$ to the target point, and (3) the direction pointing to the target point $\boldsymbol{\nu}_{\text{Im}} = (\mathbf{x}_{\text{Im}}(\mathcal{T}^{h,k}(\mathbf{x})) - \mathbf{x}) / \|\mathbf{x}_{\text{Im}}(\mathcal{T}^{h,k}(\mathbf{x})) - \mathbf{x}\|$. This signed distance together with the confidence of this measure $\delta_{\text{Im}} : \Gamma_{\text{ext}}^{h,k}(t) \rightarrow \mathbb{R}$ (locally for each surface element) will be integrated in our data assimilation framework as the data-fitting term.

² <https://gitlab.inria.fr/MoReFEM>.

2.4 Data Assimilation Strategy

We follow a sequential strategy initially proposed in [12] and further refined in [9] for the time integration procedure. This strategy has proven to be a very effective data assimilation procedure with real data for both recovering the model trajectory – hence the deformation mapping – and jointly identifying some uncertain biophysical parameters [1, 13]. Our work is here restricted to the trajectory estimation, but its originality lies in that we rely on a state-of-the-art data-fitting distance directly computed in the image sequence, instead on the distance to segmentations used in the previous papers. The principle of our data assimilation procedure is as follows. Assuming that we are at a time t^n when data are available, and that we have computed a deformation mapping $\varphi^n(\mathbf{x}) = \mathbf{x} + \mathbf{u}^n(\mathbf{x})$, we then introduce a correction step based on the data, which consists in seeking $\hat{\mathbf{u}}^n$ such that for all admissible test displacement fields $\mathbf{w} \in \mathcal{V}^{\text{ad}}$,

$$\begin{aligned} \kappa \int_{\Omega_0^{h,k}} \nabla(\hat{\mathbf{u}}^n - \mathbf{u}^n) : \mathbf{A}[\mathbf{u}^n] : \nabla \mathbf{w} \, d\Omega \\ + \gamma \int_{\Gamma_{\text{ext},0}^{h,k}} \delta_{\text{Im}}(\varphi^n)[(\hat{\mathbf{u}}^n - \mathbf{u}^n) \cdot \boldsymbol{\nu}_{\text{Im}}(\varphi^n)][\mathbf{w} \cdot \boldsymbol{\nu}_{\text{Im}}(\varphi^n)] \, d\Gamma \\ = \gamma \int_{\Gamma_{\text{ext},0}^{h,k}} \delta_{\text{Im}}(\varphi^n) \text{dist}_{\text{Im}}(\varphi^n) \cdot \mathbf{w} \, d\Gamma \end{aligned}$$

where γ is a scaling parameter for our overall data confidence, κ is a regularization parameter scaled to balance the model overall stiffness with respect to the data confidence, and $\mathbf{A}[\mathbf{u}^n]$ is the tangent stiffness tensor around the current displacement \mathbf{u}^n . We point out that this variational formulation is linear with respect to $\hat{\mathbf{u}}^n$, with a coercive bilinear form in the left-hand side. Then the model time integration is restarted from $\hat{\mathbf{u}}^n$ instead of \mathbf{u}^n . Computing successively $\mathbf{u}^{n-1} \rightarrow \mathbf{u}^n \rightarrow \hat{\mathbf{u}}^n$ is called a prediction-correction scheme. The prediction is made by the model dynamics time scheme whereas the correction is performed using the data. Note that the correction fundamentally corresponds to computing the first iteration of a quasi-Newton based minimizing procedure involving the predicted displacement field and the data-fitting term. Indeed, our sequential data assimilation procedure aims at a compromise between predicting the next displacement using the biophysical model, and minimizing the distance with respect to the new data.

2.5 Assessment Based on Displacements Extracted from Tagged MRI

Displacements from tagged MRI are extracted by using the Image Registration Toolkit library (IRTK) [18], implemented within the visualisation software Eidolon [10]. This provides full 3D displacement vectors $\mathbf{u}_{3\text{Dtag}}$ in the case of 3D tagged sequences, or their projection in the short-axis plane $\mathbf{u}_{\text{SAtag}}$ for 2D tagged MR images. By t_d we denote the time corresponding to the first frame of the tagged MR sequence (typically between 30 and 60 ms from the R

wave of QRS complex, due to the prospectively triggered tagged MRI acquisition), and relate the extracted displacements to this time instance, namely $u_{3\text{Dtag}}(\mathbf{x}, t_d) = u_{\text{SAtag}}(\mathbf{x}, t_d) = 0$. The model simulated displacements $\mathbf{u}(\mathbf{x}, t)$ are computed in the reference configuration, namely at points $\mathbf{x} \in \Omega_0^{h,k}$. Therefore, to compare them with the 3D tag, we first compute for all the model time steps t_n , the model displacement field with respect to the first tagged frame in deformed configuration:

$$\tilde{\mathbf{u}}^n : \begin{cases} \Omega^{h,k}(t) \rightarrow \mathbb{R}^3 \\ \mathbf{x} \mapsto \mathbf{u}^n((\varphi^n)^{-1}(\mathbf{x})) - \mathbf{u}^d((\varphi^n)^{-1}(\mathbf{x})) \end{cases}$$

A global discrepancy between displacements obtained from the model and data assimilation and those extracted from the 3D tagged MRI is then computed by

$$d_{3\text{D}} = \left[\sum_{n \in T_{3\text{D}}} \int_{\Omega_0^{h,k}} \|\tilde{\mathbf{u}}^n(\varphi^n(\mathbf{x}), t_n) - \mathbf{u}_{3\text{Dtag}}(\varphi^n(\mathbf{x}), t_n)\|^2 \frac{\Delta t}{T|\Omega|} d\Omega \right]^{\frac{1}{2}},$$

where $T_{3\text{D}}$ is the set of indices associated with each time when a tagged MRI is available, Δt is the time step between two tagged MR images while T is the total acquisition time, and $|\Omega|$ the total volume of ventricle. Likewise, for the subjects with only 2D tagged MRI available, we use the similarly defined measure d_{SA} . The time integration is performed only up to end-systole as the tag lines are progressively fading in the diastole.

For the quantitative comparison, the components of the errors $d_{3\text{D}}$ or $d_{2\text{DSA}}$ in the radial and circumferential directions (with respect to the prolate coordinate system local to each mesh node, defined in the model reference configuration) are used.

3 Results

Figure 1 shows the end-systolic cine MR image of a few representative subjects in the study, together with contours of two models: the initial model simulation without the data-based correction in blue, and the result of model simulation with the data-based correction in red. This qualitative comparison demonstrates that the data corrected simulation is very close to the manually segmented surfaces. Figure 2 demonstrates quantitatively the impact on errors in predicted displacements in radial and circumferential directions evaluated with respect to the displacements extracted from tagged MRI. The decrease of error in radial component confirms the qualitative analysis made from Fig. 1. The decrease of error in the circumferential component demonstrates that the corrected model was able to capture some component of the circumferential direction, which is not directly accessible from cine MRI.

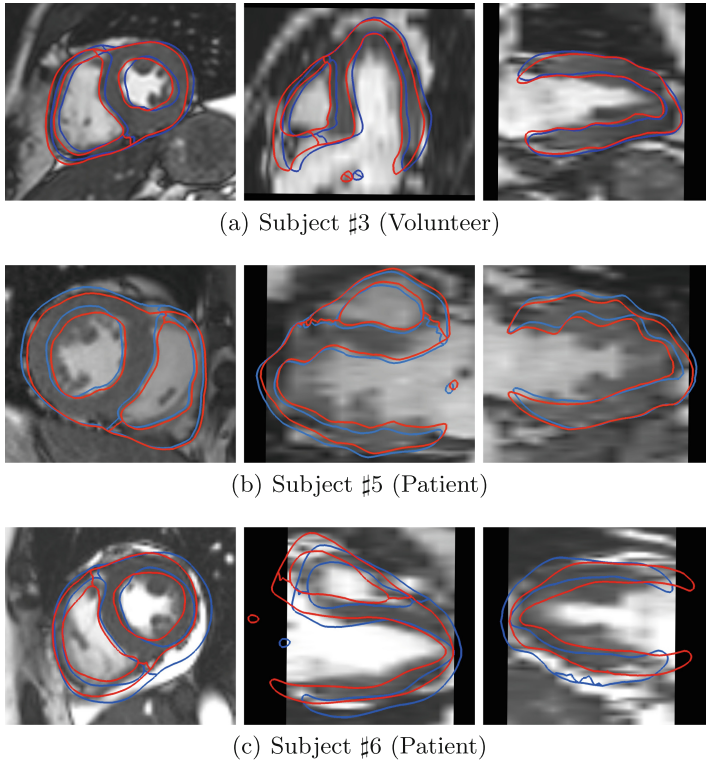


Fig. 1. Qualitative assessment of selected subjects at end-systole: comparison of the contours of the model without taking into account the data (blue) and the model corrected by the data-fitting term (red). (Color figure online)

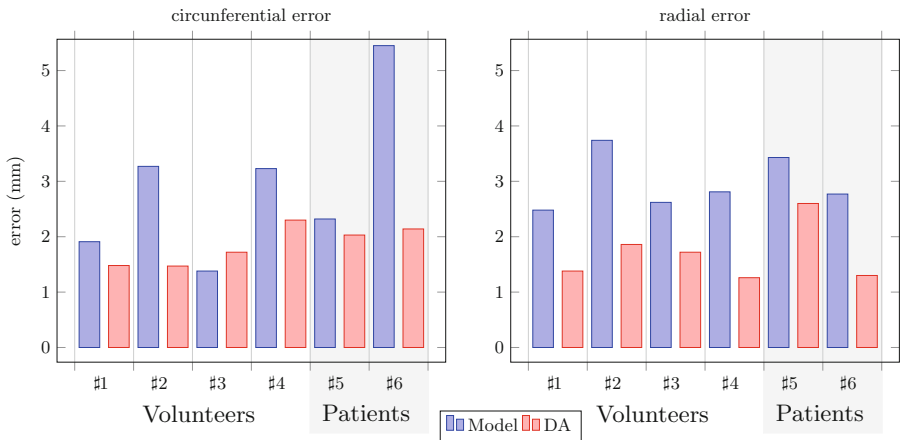


Fig. 2. Errors assessed with respect to the displacements extracted from tagged MRI. Data-free model simulation (blue) and model with data assimilation (red) (Color figure online)

4 Discussion

The datasets were acquired by two 1.5T MR systems from different vendors – Philips and Siemens – in two different clinical environments. Even though the scanning protocols were adapted to be consistent as much as possible, this nevertheless brought some challenges. First, the distance computation in cine MRI was trained only on the datasets acquired by the Philips scanner. Nevertheless, the performance was actually very good in all subjects. This is a sign that the current implementation may be directly suitable even for multi-platform and/or multi-center projects. Of course, a detailed assessment would be needed when a new type of scanner is to be included.

While 3D tagged MRI was used during the acquisition by the Philips system, only “more standard” 2D tagged MRI were acquired with Siemens (as the 3D tagged sequence was not implemented on the platform). Even though we had to adjust the quantitative verification accordingly, the comparisons of local displacements with the pseudo-ground truth (Fig. 2) showed that the model is improved in all cases (except for the circumferential component in Subject #3, where the initial model error was already small).

Additionally to MRI, the same strategy of automatic contour detection may be trained also for cine CT, and for 3D echo data. This would further increase the accessibility of 3D patient-specific cardiac models, and would be suitable even for patients contraindicated for MRI exam (e.g. non-MRI-conditional pacemakers).

The modeling setup used in this work was as in a previous project [1]. Even though the model may be improved – typically by using a more refined passive law [7,8], and a reference configuration closer to experimental data [11] – our work demonstrates that the strategy of incorporating image data in a data assimilation strategy is successful. Including more sophisticated modeling ingredients may bring further improvements, albeit we expect that this would mostly help in the estimation of myocardial properties – a natural subsequent step in our work.

5 Conclusion

A complex 3D heart model interacting with cine MRI was used to reconstruct clinically important motion indicators, which would be normally inaccessible from the given type of sequence. Secondly, a successful personalization of the model by using image data as they are acquired without any pre-segmentation paves the way for a wider use of patient-specific 3D cardiac modeling. Although the number of included subjects was limited, the data were acquired in two different clinical environments and using MRI systems from different vendors. Overall, the performed proof-of-concept work demonstrates a good potential that would justify a wider-scale pre-clinical study.

Acknowledgement. The authors acknowledge financial support from the Department of Health through the National Institute for Health Research (NIHR) comprehensive Biomedical Research Centre award to Guy's & St Thomas' NHS Foundation Trust in partnership with King's College London and the NIHR Cardiovascular MedTech Co-operative (previously existing as the Cardiovascular Healthcare Technology Co-operative 2012–2017), the support of Wellcome/EPSRC Centre for Medical Engineering [WT 203148/Z/16/Z]. The views expressed are those of the author(s) and not necessarily those of the NHS, the NIHR or the Department of Health.

References

1. Chabiniok, R., Moireau, P., Lesault, P.F., Rahmouni, A., Deux, J.F., Chapelle, D.: Estimation of tissue contractility from cardiac cine MRI using a biomechanical heart model. *Biomech. Model Mechanobiol.* **11**(5), 609–30 (2012)
2. Chapelle, D., Fragu, M., Mallet, V., Moireau, P.: Fundamental principles of data assimilation underlying the Verdandi library: applications to biophysical model personalization within euHeart. *Med. Biol. Eng. Comput.* **51**(11), 1221–1233 (2013)
3. Chapelle, D., Le Tallec, P., Moireau, P., Sorine, M.: An energy-preserving muscle tissue model: formulation and compatible discretizations. *Int. J. Multiscale Comput. Eng.* **10**(2), 189–211 (2012)
4. Ecabert, O., et al.: Automatic model-based segmentation of the heart in CT images. *IEEE Trans. Med. Imaging* **27**(9), 1189 (2008)
5. Genet, M., Stoeck, C.T., von Deuster, C., Lee, L.C., Kozerke, S.: Equilibrated warping: finite element image registration with finite strain equilibrium gap regularization. *Med. Image Anal.* **50**, 1–22 (2018)
6. Giorgi, B., Dymarkowski, S., Maes, F., Kouwenhoven, M., Bogaert, J.: Improved visualization of coronary arteries using a new three-dimensional submillimeter MR coronary angiography sequence with balanced gradients. *Am. J. Roentgenol.* **179**(4), 901–910 (2002)
7. Hadjicharalambous, M., et al.: Analysis of passive cardiac constitutive laws for parameter estimation using 3D tagged MRI. *Biomechan. Model. Mechanobiol.* **14**(4), 807–828 (2015)
8. Holzapfel, G., Ogden, R.: Constitutive modelling of passive myocardium: a structurally based framework for material characterization. *Philos. Trans. Roy. Soc. London: Math. Phys. Eng. Sci.* **367**(1902), 3445–3475 (2009)
9. Imperiale, A., Routier, A., Durrleman, S., Moireau, P.: Improving efficiency of data assimilation procedure for a biomechanical heart model by representing surfaces as currents. In: Ourselin, S., Rueckert, D., Smith, N. (eds.) *FIMH 2013*. LNCS, vol. 7945, pp. 342–351. Springer, Heidelberg (2013). https://doi.org/10.1007/978-3-642-38899-6_41
10. Kerfoot, E., et al.: Eidolon: visualization and computational framework for multimodal biomedical data analysis. In: Zheng, G., Liao, H., Jannin, P., Cattin, P., Lee, S.-L. (eds.) *MIAR 2016*. LNCS, vol. 9805, pp. 425–437. Springer, Cham (2016). https://doi.org/10.1007/978-3-319-43775-0_39
11. Klotz, S., et al.: Single-beat estimation of end-diastolic pressure-volume relationship: a novel method with potential for noninvasive application. *Am. J. Physiol. Heart Circ. Physiol.* **291**, H403–H412 (2006)
12. Moireau, P., Chapelle, D., Le Tallec, P.: Filtering for distributed mechanical systems using position measurements: perspectives in medical imaging. *Inverse Prob.* **25**(3), 035010 (2009). (25pp)

13. Moireau, P., et al.: Sequential identification of boundary support parameters in a fluid-structure vascular model using patient image data. *Biomech. Model. Mechanobiol.* **12**(3), 475–496 (2013)
14. Peters, J., Ecabert, O., Meyer, C., Kneser, R., Weese, J.: Optimizing boundary detection via simulated search with applications to multi-modal heart segmentation. *Med. Image Anal.* **14**(1), 70–84 (2010)
15. Rausch, M.K., Genet, M., Humphrey, J.D.: An augmented iterative method for identifying a stress-free reference configuration in image-based biomechanical modeling. *J. Biomech.* **58**, 227–231 (2017)
16. Rutz, A., Ryf, S., Plein, S., Boesiger, P., Kozerke, S.: Accelerated whole-heart 3D CSPAMM for myocardial motion quantification. *Magn. Reson. Med.* **59**, 755–763 (2008)
17. Sainte-Marie, J., Chapelle, D., Cimrman, R., Sorine, M.: Modeling and estimation of the cardiac electromechanical activity. *Comput. Struct.* **84**(28), 1743–1759 (2006)
18. Shi, W., et al.: A comprehensive cardiac motion estimation framework using both untagged and 3D tagged MR images based on non-rigid registration. *IEEE Trans. Med. Imaging* **31**(6), 1263–1275 (2012)